TISSUE ENGINEERING: Part C
Volume 25, Number 11, 2019

DOI: 10.1089/ten.tec.2019.0123

termis
Tissue Engineering
& Regenerative Medicine
International Society

METHODS ARTICLE

Robust and Precise Wounding and Analysis of Engineered Contractile Tissues

Sarah J. Dubois, B.Eng,[1,*] Nikita Kalashnikov, B.Eng,[1,*] and Christopher Moraes, PhD[1–3]

Fibrous tissue gap closure is a critically important process initiated in response to traumatic injury. Recent three-dimensional (3D) bioengineered models capture cellular details of this process, including wound retraction and closure, but have high failure rates, are labor-intensive, and require considerable expertise to develop and implement with tools that are typically not available in standard wet laboratories. Here, we develop a simple and effective 3D-printed wounding platform to reliably create and puncture arrays of prestressed tissues and monitor subsequent wound dynamics. We demonstrate the ability to create a range of wound sizes in a contractile collagen/fibroblast tissue, within 125 μm of the desired target location, with high degrees of circularity. Wounds exhibit an initial expansion due to tissue prestress, and sufficiently small wounds close completely within 24 h, while larger wounds initially closed much more rapidly, but did not complete the closure process. Simulating the dynamics of tissue retraction with a viscoplastic finite element model indicates a temporary elevation of circumferential stresses around the wound edge. Finally, to determine whether active wounding and retraction of the tissue significantly affect closure rates, we compared active puncture of prestressed tissue with passive removal of a structure that prevents closure, and found that active wounding and retraction substantially accelerated wound closure when compared with the passive case. Taken together, our findings support the role of active tissue mechanics in wound closure arising from an initial retraction of the tissue. More broadly, these findings demonstrate the utility of the platform and methodology developed here in further understanding the mechanobiological basis for wound closure.

Keywords: wounding, mechanobiology, viscoplasticity, contraction, remodeling

Impact Statement

In vitro models to study wound formation and closure in prestressed tissue are typically challenging to implement. This work provides an easily accessible approach to produce and analyze wounds in arrays of contractile tissues that recapitulate critical features of wound retraction and closure in animal models. The specific modeling and experiments results presented here suggest that mechanobiology effects arising from wound retraction in viscoplastic extracellular matrices could play an important role in driving wound closure.

Introduction

Fibrous tissue gap closure is a fundamental biological process needed for the proper development of various anatomical structures[1,2] such as the neural tube,[3,4] heart,[5] and palate,[6] and for tissue repair and regeneration. Damage to developed tissues initiates hemostasis, inflammation, granulation tissue formation, and remodeling in a precisely orchestrated cascade to heal the wound.[7–9] Disrupting this process leads to severe complications, including infection and prolonged inflammation.[10–12] Given the complexity of this process in humans and animals, developing *in vitro* models of gap closure is of critical importance in understanding and ultimately manipulating these biological processes.

Existing models of tissue wounding recreate various aspects of the gap closure process. In two-dimensional (2D) cultures, scratching cell monolayers with a pipette tip yields considerable insight into gap closure processes.[13–17] More

Departments of [1]Chemical Engineering and [2]Biological and Biomedical Engineering, McGill University, Montreal, Canada.
[3]Goodman Cancer Research Center, McGill University, Montreal, Canada.
*Both these authors contributed equally to this work.

advanced approaches such as laser ablation[18,19] may also be used. Alternatively, the wound can be premade using stencil[20–23] or tissue patterning techniques.[24–26] However, these strategies do not capture the mechanical complexities of a three-dimensional (3D) wound, which may be of critical importance.

The 3D models of fibrous tissues can be engineered to recreate various stromal tissues,[27–30] and these can be adapted for wound models. Wound-like inclusions have been created during fabrication,[31–34] but this approach does not capture *in vivo*-like features of wounding, including retraction of the wound edge in tissues under tension.[35] To address these issues, Sakar and colleagues recently developed a 3D bioengineered wounding model, in which fibroblast/collagen tissues contract around anchoring pillars to form prestressed microtissues[36–39] that were then microsurgically injured using a robotically controlled micromanipulator.[40] This model recreates tissue prestress, exhibits wound retraction, and closes over time, and provides insight into the mechanics underlying wound closure.

Here, we address technical challenges that limit the widespread utility of the model developed by Sakar *et al.* Their system requires manual micromanipulation of the wounding tool to perform layer-by-layer sequential dissection, using visual feedback. This requires considerable skill and expertise, and would not be scalable for higher throughput applications, without advanced robotics and control feedback loops that are generally inaccessible in standard wet laboratories. To address these issues, we develop a versatile and readily implemented 3D-printed wounding apparatus, in which arrayed prestressed contractile tissues are punctured with a self-aligning array of needles at predefined locations. Using this platform, we can rapidly create punctures in prestressed tissues at precise locations and generate wounds in a plate of 24 tissues within 1 min. This platform allows us to readily observe wound formation, retraction, and closure; infer mechanical characteristics of the contracted collagen matrix from these data; and demonstrate that tissue retraction mechanically directs future wound closure.

Materials and Methods

Unless otherwise stated, all cell culture materials and supplies were purchased from Fisher Scientific (Ottawa, ON) and chemicals from Sigma-Aldrich (Oakville, ON).

Tissue wounding platform fabrication

The tissue culture portion of the device containing anchoring micropillars was fabricated using 3D printing, soft lithography, and double-replica molding in polydimethylsiloxane (PDMS). Master molds were designed and printed with an Ember 3D printer (Autodesk) in PR57-K Black Prototyping Resin. The 3D-printed parts were washed in isopropanol, fully cured under a 36 W ultraviolet (UV) light for at least 12 h, and spray-treated with a mold release agent (Mann Ease Release 200 Agent; Smooth-On, East Texas, PA). PDMS prepolymer (Sylgard 184; Dow Corning) was degassed, loaded, and cured at 70°C for 4 h to produce the negative replica molds. A double replication step was performed, using a passivation layer of tridecafluoro-1,2,2-tetrahydrooctyle)-1-trichlorosilane (Gelest, Morrisville, PA) deposited in vapor phase to facilitate release. Fabricated devices were mounted in six-well plates, cured, and sterilized under UV light for 2 h. A second device was printed to fit the culture substrate, with positioned holes for wounding needles. Selected needles were mounted in the device, or alternatively, the through-hole can be left open as a guide to insert selected needles when needed.

Tissue formation and imaging

Human bone marrow fibroblasts (HS-5; ATCC) were used as a model contractile fibroblast cell. HS-5s were cultured in Dulbecco's modified Eagle's medium (DMEM; Gibco), supplemented with 10% fetal bovine serum and 1% antibiotic/antimycotic, at 37°C and 5% CO_2. Solubilized collagen (Advanced BioMatrix), 10×DMEM, sodium bicarbonate buffer, and sterile water were mixed following the manufacturer's instructions, and titrated to neutral pH with 1 M sodium hydroxide. Trypsinized cells were added at final concentrations of 3 million cells/mL in 1.5 mg/mL collagen. Gels were pipetted into each device and gelled for 1 h at 37°C. Media were added, and the gels contracted over 48 h around the anchoring pillars. The wounding platform was then positioned using the guide structures and pressed down to puncture the tissues. At selected time points, tissues were fixed (4% paraformaldehyde, 3 h), permeabilized (0.1% Triton-X, 45 min), labeled (FITC-phalloidin), and/or imaged using brightfield or fluorescent microscopy. Analysis was performed using ImageJ (NIH) to quantify wound area, position, and circularity.

Finite element modeling

To develop estimates of stress patterns surrounding the wound during retraction, a 2D axisymmetric model was implemented in COMSOL (Burlington, MA; model details provided in Supplementary Data), and the inverse finite element method was used to determine a material model formulation and material parameters that match observations of wound expansion after puncture. Linear elastic, viscoelastic, and viscoplastic deformation models (parameters in Fig. 4C) were tested using this approach. Briefly, linear elastic and viscoelastic models are described by an elastic modulus E_e, without/with viscous modulus E_v and viscosity μ. The viscoelastic model is extended to incorporate viscoplastic behavior by adding a viscosity term with a yield stress threshold, and a softening function to reduce yield stress under constant material loading.[41] Viscoplasticity is described with a linear Norton/Hoff model:

$$\frac{d\varepsilon_{viscoplastic}}{dt} = A\sigma^{n}_{viscoplastic} = \frac{1}{\mu}\sigma_{viscoplastic}$$

where the exponent n is set to 1 as per the perfect viscoplastic assumption and the viscoplastic rate coefficient A is selected to be the inverse of viscosity μ. Initial material parameters for these models were obtained from literature sources for mechanical characterization of cell-laden collagen hydrogels.[38,41–43] For all models, tissue prestress is introduced by applying a positive radial displacement boundary condition to match the collagen pull-away distance observed at the micropillars. Tissue wounds are initiated by setting the material properties of a central ''hole''

to zero. Further details describing the finite element methods and assumptions applied are available as Supplementary Data.

Results and Discussion

Fabrication and wounding of prestressed tissue arrays

Suspended tissue arrays were fabricated by casting a collagen/cell mixture into a PDMS-based device with integrated anchoring pillars. PDMS devices containing arrays of pillars in square formations (Fig. 1A) were readily fabricated using the described 3D printing/double replica molding process, and were designed to have four 600 μm tall pillars of 500 μm diameter, with center-to-center spacings of 2.5 mm. Contractile tissues were formed by gelling 14 μL of a cell gel solution in each chamber.

Tissues contract over 48 h to produce a characteristic dense fibrous band around the pillars (Fig. 1B). This dense region arises from free contraction of the unanchored collagen between the edge of the well and the pillars. Central cells pull the collagen tissues toward the tissue center, as evidenced by collagen pull-away from the pillar edges. Simple pillars allowed the tissue to slip over their tips during contraction. Seven hundred micrometer-diameter spheres atop each pillar were large enough to anchor the tissues over 4–5 days, and sufficiently small to allow PDMS release during replica molding.

The wounding platform fits over the tissues using alignment grooves built into the culture device (Fig. 1C). With these grooves to automatically guide box positioning, the wounding array punctured each tissue at predefined positions. Manually pressing the structure down was sufficient to align the platform and puncture the tissue (Fig. 1D, E). For all experiments described here, we created wounds in the center of each tissue. Improper wound positioning often leads the development of uneven stresses within the tissue, which can lead to premature tissue failure, and positioning wounds at the center of each tissue avoids this concern. However, wound positioning can also be defined arbitrarily, if needed to answer specific questions that require targeted placement of defects within a tissue. For example, this would be relevant for more complex engineered tissue models that incorporate multiple cell types or advanced structures.

Characteristic wound dimensions

We empirically found that standard pointed needles often did not create a wound, likely because their tips are thin and relatively rounded, and cause local compaction of the soft collagen tissue. Filing the needles flat (Fig. 2A) and selecting a depth that forces them to penetrate into the underlying PDMS surface reliably produced open wounds as needed. Hence, successful wounding is often accompanied by necessary damage to the underlying PDMS surface.

Needle diameters of 400–900 μm (representative images in Fig. 2A) were selected for these studies. The majority of all wounds formed were within 125 μm of the desired location (or 5% of the tissue linear dimension) (Fig. 2B). In some cases, wounds were observed within 10% of the desired location, likely due to slight variations in device dimensions arising from PDMS shrinkage during the multiple replica molding steps.[44] All wounds produced had circularity shape factors within 10% of a perfect circle, with no significant differences observed based on needle size (Fig. 2C). Wound area was significantly influenced by needle size (Fig. 2D). Interestingly, for small-diameter needles, all wounds were larger than the cross-sectional area of the needle, suggesting that the tissue is pulling away or retracting after puncture, as expected in a prestressed and physiologically realistic wound model.[35] When testing larger needle diameters, although the majority of wounds were larger than the puncturing needle, some were smaller than expected, suggesting incomplete wounding with larger needles. This is likely dependent on the quality of the needle tip, and filing a cookie-cutter edge into larger needles should improve these results.

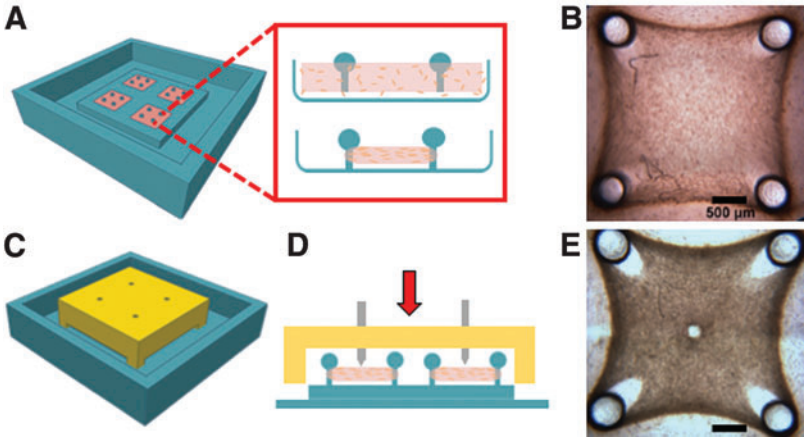

FIG. 1. Overview of engineered tissue wounding platform. **(A)** Schematic overview of tissue culture device operation. Cell-laden collagen is loaded into PDMS wells containing replica-molded 3D-printed anchoring pillars, which then contracts to form a prestressed tissue suspended between the pillars. **(B)** Representative brightfield image of prestressed tissue (scale bar = 500 μm). **(C)** Schematic overview of the wounding device operation. A 3D-printed structure with integrated needles is designed to fit over positioning grooves in the culture substrate, precisely locating the needles at defined locations over the engineered tissues. **(D)** Manually pressing the wounding platform down creates **(E)** well-defined and precisely positioned holes in the collagen tissues (scale bar = 500 μm). 3D, three-dimensional; PDMS, polydimethylsiloxane. Color images are available online.

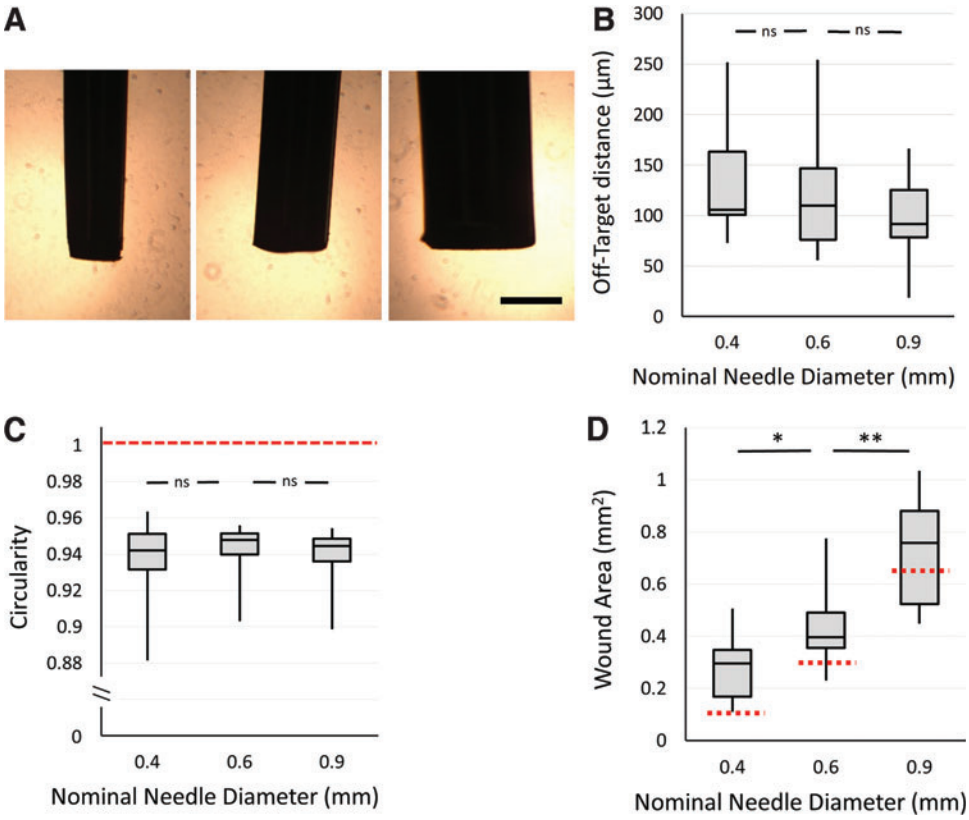

FIG. 2. Characterization of tissue wounding performance. **(A)** Brightfield microscopy image of selected punching needles, with nominal diameters of 0.4, 0.6, and 0.9 mm (scale bar = 500 μm). **(B)** Off-target distance of the wound center from the targeted position. When applied to tissues with lengths of 2500 μm, the majority of wounds are within 5% of their desired positions. **(C)** Circularity of produced wounds did not vary based on needle size. The *red dashed line* indicates a perfectly circular wound. **(D)** Areas of wounds created in the centers of engineered tissues based on selected needle diameters. *Red dashed lines* represent the expected wound size corresponding to the needle cross-sectional area. All data represented as box plots showing median interquartile range and range ($n = 11–16$; $^*p < 0.05$, $^{**}p < 0.001$, n.s. $p > 0.3$ by two-tailed ANOVA with Tukey *post hoc* comparison). ANOVA, analysis of variance. Color images are available online.

Wound closure

Small wounds (<250 μm) closed within 24–48 h, while larger wounds (>750 μm diameter) remained open even 96 h postwounding (Fig. 3A, B). We qualitatively examined cell behavior at the wound edges during closure by fluorescently labeling cells in fixed tissues (Fig. 3C, D) and noticed that ''bridging'' strings of actin-positive cells formed across the gap in the final stages of closure, consistent with previous studies.[40] These qualitative observations demonstrate that the tissue models developed here, despite being significantly larger than existing microtissue models, still capture relevant physiological phenomena during gap closure.

To determine whether wounds size affects closure dynamics in these models, closure speeds were analyzed based on initial wound size (Fig. 3E, F). Although larger wounds did not fully close, the initial closure speeds for wounds >750 μm in diameter were significantly faster than those of smaller wounds (Fig. 3F). Larger wound sizes within this group generally produced faster closure rates (individual data points presented in Supplementary Fig. S1). This suggests that distinct closure mechanisms may be activated in large and small wounds. Speculatively, the increased closure rates may be due to the mechanical activation of the dense, aligned fibrous tissue band surrounding the anchoring pillars while making large wounds.

In the microtissue models presented by Sarkar *et al.*, the dense collagen bands formed at the tissue periphery constitute a substantial portion of the tissue, and even the smallest wounds alter global tissue dimensions. Since global tissue size also changes during re-establishment of homeostatic tension, the authors conclude that wound closure arises from a combination of global tissue remodeling and local tissue dynamics (Fig. 3G). To determine if this was also true in our system, we compared tissue dimensions in wounded and unwounded models during closure, and found no changes arising from wounding (Fig. 3H). Hence, we can conclude that the present model system provides a sufficiently flexible design space to produce small enough wounds in sufficiently large tissues to effectively decouple local and global remodeling activity, to better understand these distinct processes.

Analysis of wound edge retraction

Wound edge retraction and stabilization are known to occur when puncturing a prestressed tissue, as in animal models (Fig. 4A).[35] Hence, we characterized small wound

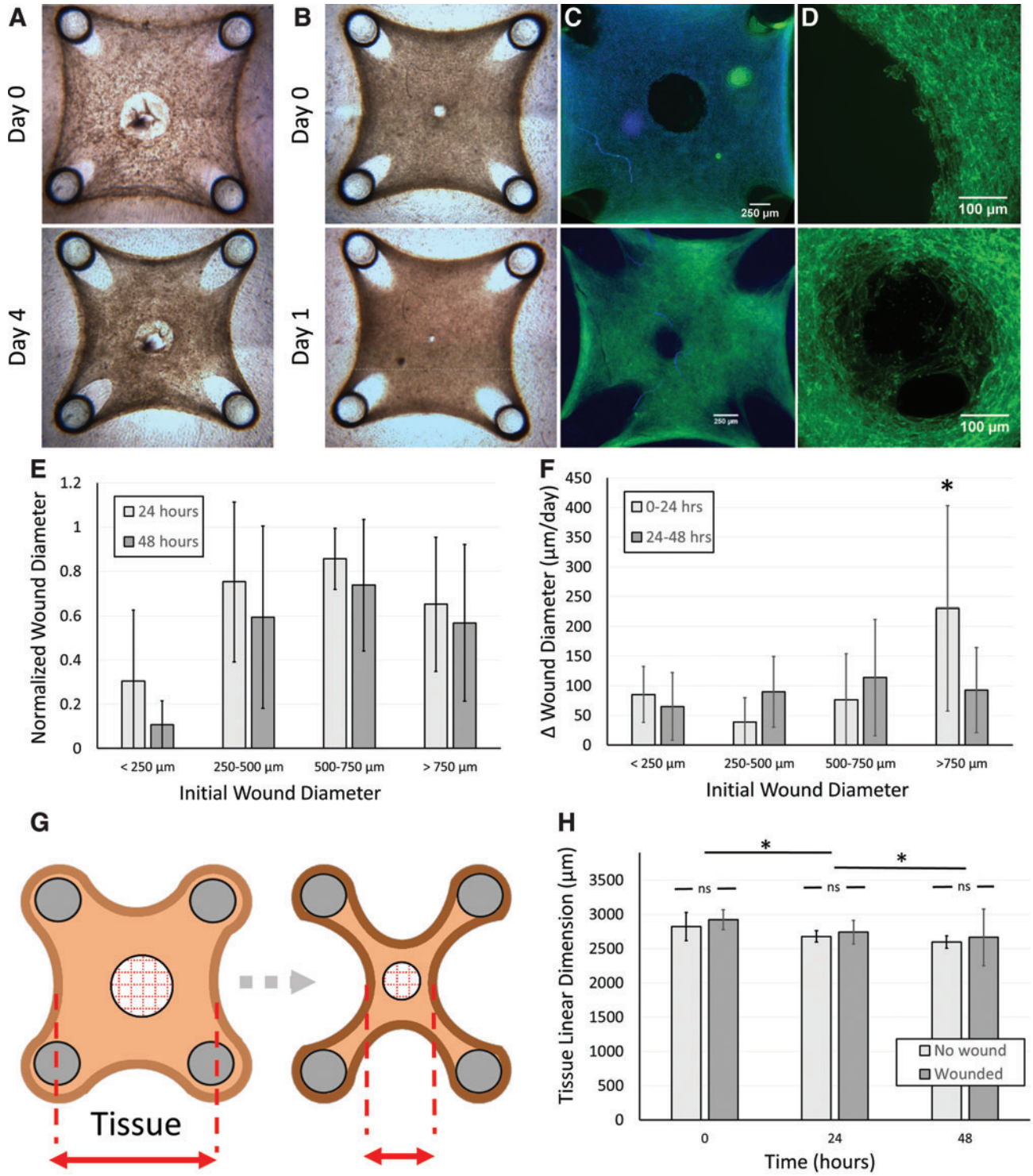

FIG. 3. Wounds and tissue closure characteristics. **(A, B)** Representative images of wounded engineered tissues with **(A)** large and **(B)** small punctures immediately after wounding and during closure at days 1 and 4. **(C, D)** Fluorescent micrographs of the **(C)** wound and **(D)** wound edge immediately after puncture (*top panels*) and after 24 h (*bottom panels*; *green* = F-actin). Scale bars = 250 µm for **(C)** and 100 µm for **(D)**. **(E, F)** Characteristic wound dimensions over 2 days of closure for wounds grouped based on initial size, expressed as **(E)** wound diameter normalized to the initial wound size and **(F)** daily change in wound diameter over the 0–24- and 24–48-h periods after wounding. Data demonstrate that small wound areas close rapidly, but the linear closure rate is similar across days and initial wound size, except for a significant increase in closure rate for the largest wounds tested. **(G)** Schematic representation of the potential relationship between changing tissue dimensions and wound closure. Coordinated movement of the whole tissue may assist in wound closure as the tissue continues to contract, and this effect would be influenced by the relative size of the wound compared with the size of the tissue. **(H)** Comparison of linear tissue dimensions between wounded and unwounded model tissues during further tissue contraction and wound closure. All data reported as mean ± standard deviation ($n = 10–18$) in **(E, F, H)**; (*$p < 0.01$, by two-tailed ANOVA with Tukey *post hoc* comparisons). Color images are available online.

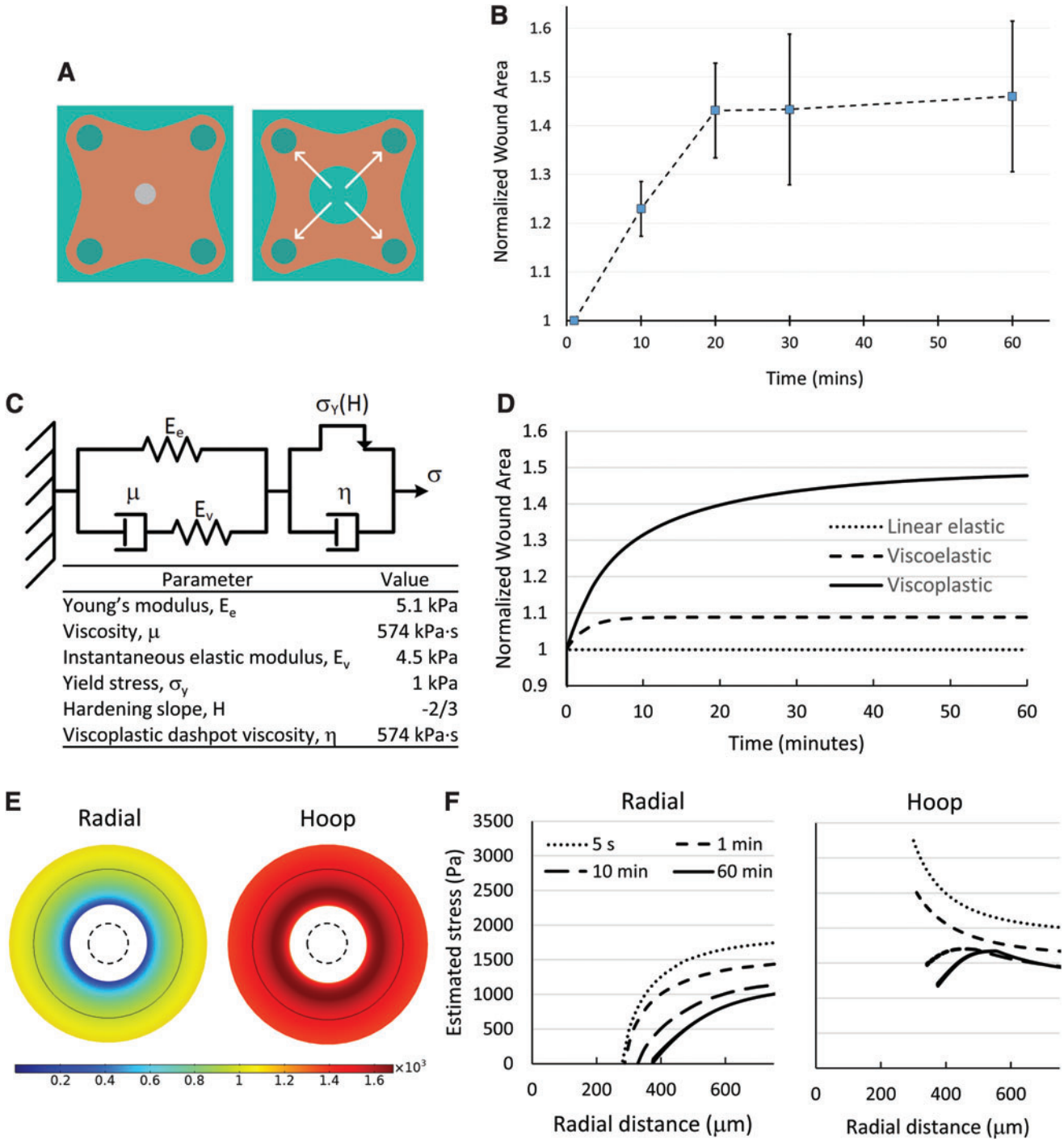

FIG. 4. Wound retraction following tissue puncture and associated finite element model. **(A)** Wound retraction due to tissue prestress. **(B)** Temporal evolution of wound area normalized to initial wound size after tissue puncture. **(C)** Viscoplastic material model and associated parameters to simulate wound retraction. **(D)** Comparison of simulated wound retraction for simple linear elastic, viscoelastic, and combined viscoplastic models. **(E)** Characteristic radial and hoop stresses established after complete wound retraction. *Dashed lines* indicate initial wound size immediately after tissue puncture. **(F)** Spatial radial and hoop stress profiles within the tissues over time. Wounding causes a reduction in radial stress near the wound edge and a corresponding transient increase in hoop stress. Viscoplastic stress dissipation works over time to attenuate both stress profiles, leaving a characteristic hoop stress peak near the wound. Color images are available online.

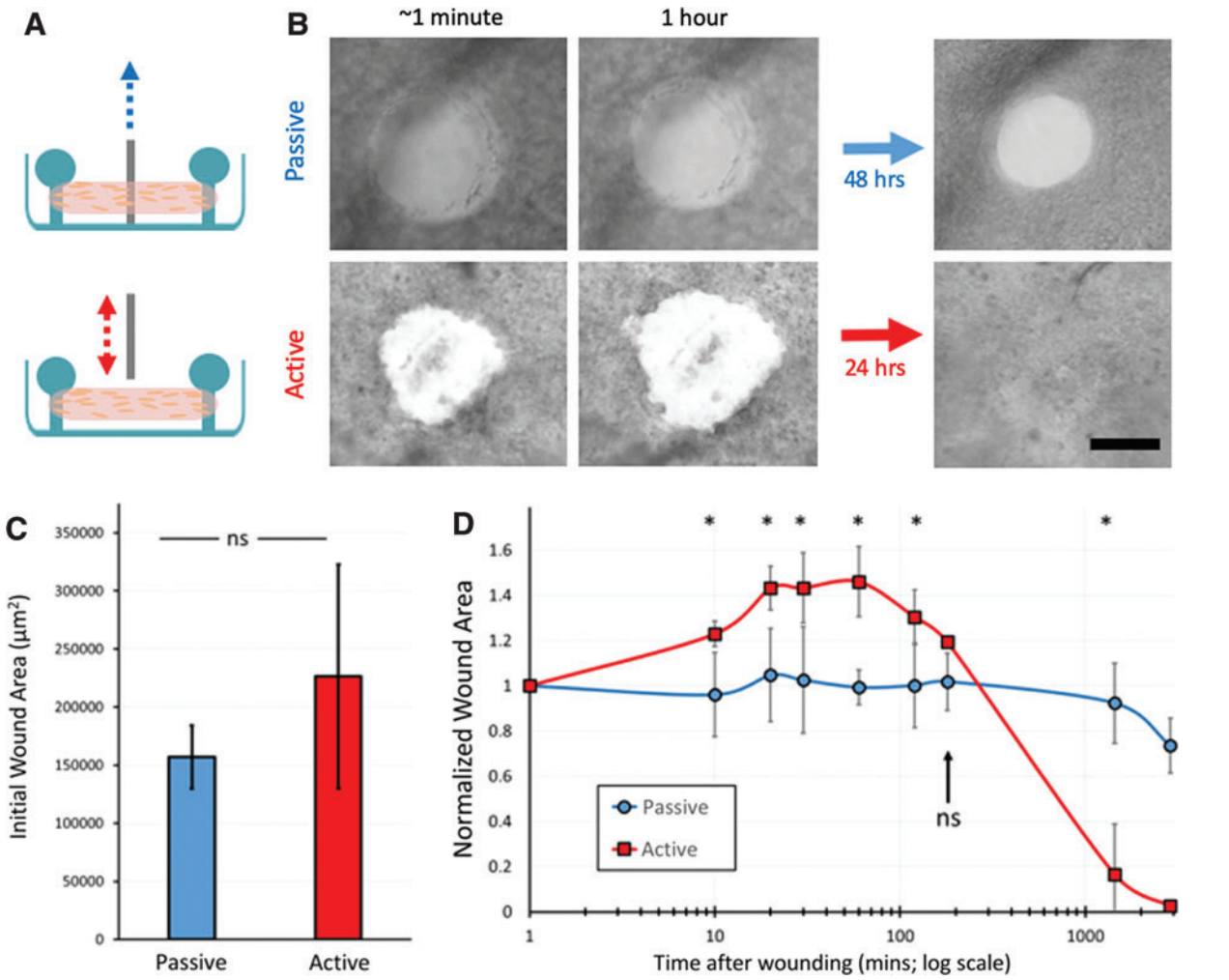

FIG. 5. Comparison between passive and active wounding. **(A)** Tissues were either passively wounded by removing an obstruction from the tissue or actively wounded with the 3D-printed wounding device to achieve small wounds. **(B)** Passively formed wounds partially closed within 48 h, but actively formed wounds first expanded and then closed completely within 24 h (scale bar = 250 μm). **(C)** No significant differences observed in initial wound area between the passive and active wounding techniques immediately after tissue puncture. **(D)** Analysis of wound area normalized to initial wound area over time. Passively generated wounds started to close after 24 h, while actively formed wounds first expanded over the first 1 h and then rapidly closed within 24 h ($n = 4$–6, $^*p < 0.05$, n.s. $p > 0.10$, by two-tailed ANOVA with Tukey *post hoc* comparisons). Color images are available online.

retraction dynamics in our system. Wounds grew in size for ~20 min, and stabilized at 1.4× the initial wound area (Fig. 4B). Some heterogeneity was observed, suggesting that variability in tissue mechanics does exist between samples.

We then asked whether our observations of wound retraction could allow us to identify a material model that would provide insight into the mechanical stress patterns surrounding the wound. We developed finite element analyses for linear, viscoelastic, and viscoplastic materials (Fig. 4C) using values obtained from literature.[38,41–43,45] Linear elastic material models did not exhibit time-dependent retraction, as the wound instantly expanded to release tissue stress. While viscoelastic models did improve on this and capture time-dependent wound expansion (Fig. 4D), they did not capture the wound expansion magnitude observed experimentally (Fig. 4B). Recently, collagen tissues have been shown to exhibit viscoplastic behaviors,[41,43,46–48] and hence, we implemented stress-dependent plasticity (Fig. 4C) into our analysis. This material model successfully matched both the magnitude and time dependency of the wound opening, utilizing parameters similar to those obtained from fundamental mechanical characterization studies of cell-densified collagen (listed in Fig. 4C).[38,41–43]

After confirming realistic strain behavior, we used the viscoplastic simulations to determine whether stress patterns should occur around the wound retraction sites (Fig. 4E, F). Wounding causes immediate reductions in radial stress from the baseline tissue stress levels (2 kPa), and a transient increase in circumferential hoop stress that extends into the surrounding tissue. Viscoplastic deformation dissipates stress over time, but circumferential hoop stress variations remain significant and elevated near the wound for more than 1 h during and after retraction.

The finite element models presented here do have significant limitations in terms of the precision of predicted

stress values. For example, the models are based on material parameters obtained from the literature and hence do not accurately capture absolute stress levels present in these tissues. The patterns of stress around the wound should remain valid. Furthermore, the model assumes homogenous mechanical properties in the area surrounding the wound tissue, which is quite unlikely given the large area retraction observed that must change local mechanical properties. Hence, these modeling results should only serve to validate that persistent circumferential hoop stress variations arise and are maintained for a long time period after wounding. Given that cells are known to contract in response to applied tensional stress and stress gradients,[49] and that circumferential hoop stresses form the basis for purse-string-based wound closure,[50] this insight into stress patterns around the wound leads to the intriguing speculation that transient stresses during wound retraction may affect wound closure in a manner dictated by highly localized tissue stress patterns at the wound edge.

Wound closure dynamics in response to active and passive wounding

To support the hypothesis that mechanical stress developed around the wound during retraction influences closure dynamics, we compared active wounding of a prestressed 3D tissue, in which wound retraction is expected, with passive removal of an object that obstructs wound closure (Fig. 5A). This has previously been shown to affect tissue mechanics and closure in 2D systems,[51] and our model is uniquely suited to compare these cases. While actively wounded tissues rapidly closed within 24 h, passively wounded tissues did exhibit signs of wound edge smoothing and closure, but did not close within 48 h (Fig. 5B). We verified that wound dimensions produced in both models were similar (Fig. 5C) and noted that greater heterogeneity in wound sizes was observed in actively wounded tissues due to variable retractions at the wound edge.

To quantify both retraction and wound closure, we normalized measured wound area to the initial wound. These experiments confirm that passive tissues do not exhibit retraction, while active tissues rapidly retract and then rapidly close (Fig. 5D). These results strongly suggest that the retraction process itself activates rapid wound closure, perhaps through mechanical activation of cells around the wound. Unlike standard epithelial scratch-based wound closure assays, cell proliferation is unlikely to play a role over these timescales, given the established low proliferation rates of fibroblast cells in 3D matrices[52] and recent findings that cell contractility and not proliferation acts to close wounds in 3D fibrous tissues.[40] A mechanical basis for rapid closure is also conceptually consistent with recent studies demonstrating that cells can migrate through a matrix via a slingshot action, in which tension is first built up by tissue deformation, and the elastic energy stored in the matrix can be directed on release of cell adhesion to enhance migration rates.[53] Analogously, actively wounding the tissue causes retraction at the wound edge, which increases local matrix density, stiffness, and circumferential hoop stress (Fig. 3E, F). Speculatively, these factors could act to mechanically activate cells in this region to contract and migrate, thus rapidly closing the gap.

System utility and limitations

At present, the contracted collagen system developed by Sakar *et al.*[40] remains the only *in vitro* platform to study wounding and recovery in fibrous tissues that capture retraction of the wound edge, a common feature of human and animal model wounds in traumatic injury and developmental morphogenesis. We anticipate that more complex culture systems will be developed, based on a prestressed tissue, that incorporate epithelial layers, alternative matrix compositions, or multiple cell types. These advanced models would allow investigation into more realistic models of wound healing, including cellular processes, such as proliferation, that play a minimal role in fibrous tissue closure, but are more important in epithelial closure mechanisms. The puncture platform developed in this work should be broadly applicable to support these advances, provided that the tissues remain sufficiently soft to allow puncture. The primary limitations associated with this strategy would be around the relative sizing and mechanical characteristics of both the tissue models and the puncturing needle. If the desired wound is too small, a fine needle might simply pierce a low-stress tissue without coring it, allowing it to seal up rapidly much like a rubber septum. Higher levels of tissue stress would force the tissue to spring apart at the wound, addressing this issue. Fine needles may also flex during operation, which could lose wounding efficiency or reduce positional accuracy. While this potential concern may be partially addressed by selecting mechanically rigid materials for the needle, it still presents a fundamental limitation to the minimum wound size possible with this approach.

Conclusions

We have developed an easily implemented and readily accessible tissue-engineered model system to study fibrous tissue wounding and closure. The 3D-printed system to puncture prestressed contractile tissues in predefined positions can be constructed with resources that are readily available at most research institutions. Although the system does not provide the spatial resolution of techniques such as microsurgery or laser ablation, the system does significantly improve experimental ease and throughput, affords the capacity to manipulate wound size, and captures key features of wounding and recovery in animal models. The system can be sized appropriately to isolate the effects of local wound healing from global tissue remodeling. Observations of wound retraction in these models provide insight into the mechanical viscoplastic state of the tissue, which suggests that transient mechanical stresses during wound retraction may influence wound closure rates. Taken together, these results demonstrate that this simple technological method can be used to further develop insight into this biologically critical process.

Acknowledgment

Access to computational modeling software provided by CMC Microsystems.

Disclosure Statement

The authors declare no conflict of interest.

Funding Information

This project was funded by the Natural Sciences and Engineering Research Council of Canada (NSERC; Discovery RGPIN-2015-05512), the Fonds de recherche du Quebec—Nature et technologies (FRQNT; Grant No. 205292), and the Canada Research Chairs program in Advanced Cellular Microenvironments to C.M. S.J.D. and N.K. gratefully acknowledge support from NSERC and the Eugenie Ulmer Lamothe fund.

Supplementary Material

Supplementary Data
Supplementary Figure S1

References

1. Pérez-Pomares, J.M., and Foty, R.A. Tissue fusion and cell sorting in embryonic development and disease: biomedical implications. Bioessays **28,** 809, 2006.
2. Ray, H.J., and Niswander, L. Mechanisms of tissue fusion during development. Dev Camb Engl **139,** 1701, 2012.
3. Ybot-Gonzalez, P., Savery, D., Gerrelli, D., *et al.* Convergent extension, planar-cell-polarity signalling and initiation of mouse neural tube closure. Development **134,** 789, 2007.
4. Pyrgaki, C., Trainor, P., Hadjantonakis, A.-K., and Niswander, L. Dynamic imaging of mammalian neural tube closure. Dev Biol **344,** 941, 2010.
5. Lamers Wouter, H., and Moorman Antoon, F.M. Cardiac septation. Circ Res **91,** 93, 2002.
6. Bush, J.O., and Jiang, R. Palatogenesis: morphogenetic and molecular mechanisms of secondary palate development. Development **139,** 231, 2012.
7. Martin, P. Wound healing—aiming for perfect skin regeneration. Science **276,** 75, 1997.
8. Singer, A.J., and Clark, R.A.F. Cutaneous wound healing. N Engl J Med **341,** 738, 1999.
9. Gurtner, G.C., Werner, S., Barrandon, Y., and Longaker, M.T. Wound repair and regeneration. Nature **453,** 314, 2008.
10. Robson, M.C. Wound infection: a failure of wound healing caused by an imbalance of bacteria. Surg Clin North Am **77,** 637, 1997.
11. Stadelmann, W.K., Digenis, A.G., and Tobin, G.R. Impediments to wound healing. Am J Surg **176**(Suppl 1), 39S, 1998.
12. Qian, L.-W., Fourcaudot, A.B., Yamane, K., You, T., Chan, R.K., and Leung, K.P. Exacerbated and prolonged inflammation impairs wound healing and increases scarring. Wound Repair Regen **24,** 26, 2016.
13. Bement, W.M., Forscher, P., and Mooseker, M.S. A novel cytoskeletal structure involved in purse string wound closure and cell polarity maintenance. J Cell Biol **121,** 565, 1993.
14. Fenteany, G., Janmey, P.A., and Stossel, T.P. Signaling pathways and cell mechanics involved in wound closure by epithelial cell sheets. Curr Biol **10,** 831, 2000.
15. Omelchenko, T., Vasiliev, J.M., Gelfand, I.M., Feder, H.H., and Bonder, E.M. Rho-dependent formation of epithelial ''leader'' cells during wound healing. Proc Natl Acad Sci U S A **100,** 10788, 2003.
16. Grasso, S., Hernández, J.A., and Chifflet, S. Roles of wound geometry, wound size, and extracellular matrix in the healing response of bovine corneal endothelial cells in culture. Am J Physiol Cell Physiol **293,** C1327, 2007.
17. Liang, C.-C., Park, A.Y., and Guan, J.-L. In vitro scratch assay: a convenient and inexpensive method for analysis of cell migration in vitro. Nat Protoc **2,** 329, 2007.
18. Tamada, M., Perez, T.D., Nelson, W.J., and Sheetz, M.P. Two distinct modes of myosin assembly and dynamics during epithelial wound closure. J Cell Biol **176,** 27, 2007.
19. Brugués A, Anon, E., Conte, V., *et al.* Forces driving epithelial wound healing. Nat Phys **10,** 683, 2014.
20. Poujade, M., Grasland-Mongrain, E., Hertzog, A., *et al.* Collective migration of an epithelial monolayer in response to a model wound. Proc Natl Acad Sci U S A **104,** 15988, 2007.
21. Anon, E., Serra-Picamal, X., Hersen, P., *et al.* Cell crawling mediates collective cell migration to close undamaged epithelial gaps. Proc Natl Acad Sci U S A **109,** 10891, 2012.
22. Cochet-Escartin, O., Ranft, J., Silberzan, P., and Marcq, P. Border forces and friction control epithelial closure dynamics. Biophys J **106,** 65, 2014.
23. Ravasio, A., Cheddadi, I., Chen, T., *et al.* Gap geometry dictates epithelial closure efficiency. Nat Commun **6,** 7683, 2015.
24. Vedula, S.R.K., Hirata, H., Nai, M.H., *et al.* Epithelial bridges maintain tissue integrity during collective cell migration. Nat Mater **13,** 87, 2014.
25. Nier, V., Deforet, M., Duclos, G., *et al.* Tissue fusion over nonadhering surfaces. Proc Natl Acad Sci U S A **112,** 9546, 2015.
26. Vedula, S.R.K., Peyret, G., Cheddadi, I., *et al.* Mechanics of epithelial closure over non-adherent environments. Nat Commun **6,** 6111, 2015.
27. Bell, E., Ivarsson, B., and Merrill, C. Production of a tissue-like structure by contraction of collagen lattices by human fibroblasts of different proliferative potential in vitro. Proc Natl Acad Sci U S A **76,** 1274, 1979.
28. Moraes, C., Simon, A.B., Putnam, A.J., and Takayama, S. Aqueous two-phase printing of cell-containing contractile collagen microgels. Biomaterials **34,** 9623, 2013.
29. Carlson, M.A., and Longaker, M.T. The fibroblast-populated collagen matrix as a model of wound healing: a review of the evidence. Wound Repair Regen **12,** 134, 2004.
30. Leung, B.M., Moraes, C., Cavnar, S.P., Luker, K.E., Luker, G.D., and Takayama, S. Microscale 3D collagen cell culture assays in conventional flat-bottom 384-well plates. J Lab Autom **20,** 138, 2015.
31. Safferling, K., Sütterlin, T., Westphal, K., *et al.* Wound healing revised: a novel reepithelialization mechanism revealed by in vitro and in silico models. J Cell Biol **203,** 691, 2013.
32. Chen, Z.J., Yang, J.P., Wu, B.M., and Tawil, B. A novel three-dimensional wound healing model. J Dev Biol **2,** 198, 2014.
33. Price, B.L., Lovering, A.M., Bowling, F.L., and Dobson, C.B. Development of a novel collagen wound model to simulate the activity and distribution of antimicrobials in soft tissue during diabetic foot infection. Antimicrob Agents Chemother **60,** 6880, 2016.
34. Ottosson, M., Jakobsson, A., and Johansson, F. Accelerated wound closure—differently organized nanofibers affect cell migration and hence the closure of artificial wounds in a cell based in vitro model. PLoS One **12,** e0169419, 2017.
35. Davidson, J.M. Animal models for wound repair. Arch Dermatol Res **290**(Suppl), S1, 1998.

36. Legant, W.R., Pathak, A., Yang, M.T., Deshpande, V.S., McMeeking, R.M., and Chen, C.S. Microfabricated tissue gauges to measure and manipulate forces from 3D microtissues. Proc Natl Acad Sci U S A **106,** 10097, 2009.
37. Legant, W.R., Chen, C.S., and Vogel, V. Force-induced fibronectin assembly and matrix remodeling in a 3D microtissue model of tissue morphogenesis. Integr Biol **4,** 1164, 2012.
38. Wang, H., Svoronos, A.A., Boudou, T., *et al.* Necking and failure of constrained 3D microtissues induced by cellular tension. Proc Natl Acad Sci U S A **110,** 20923, 2013.
39. Ramade, A., Legant, W.R., Picart, C., Chen, C.S., and Boudou, T. Chapter 13—Microfabrication of a Platform to Measure and Manipulate the Mechanics of Engineered Microtissues. Methods Cell Biol **121,** 191–211, 2014.
40. Sakar, M.S., Eyckmans, J., Pieters, R., Eberli, D., Nelson, B.J., and Chen, C.S. Cellular forces and matrix assembly coordinate fibrous tissue repair. Nat Commun **7,** 11036, 2016.
41. Malandrino, A., Trepat, X., Kamm, R.D., and Mak, M. Dynamic filopodial forces induce accumulation, damage, and plastic remodeling of 3D extracellular matrices. PLoS Comput Biol **15,** e1006684, 2019.
42. Feng, Z., Seya, D., Kitajima, T., Kosawada, T., Nakamura, T., and Umezu, M. Viscoelastic characteristics of contracted collagen gels populated with rat fibroblasts or cardiomyocytes. J Artif Organs **13,** 139, 2010.
43. Liu, A.S., Wang, H., Copeland, C.R., Chen, C.S., Shenoy, V.B., and Reich, D.H. Matrix viscoplasticity and its shielding by active mechanics in microtissue models: experiments and mathematical modeling. Sci Rep **6,** 33919, 2016.
44. Moraes, C., Sun, Y., and Simmons, C.A. Solving the shrinkage-induced PDMS alignment registration issue in multilayer soft lithography. J Micromech Microeng **19,** 065015, 2009.
45. Raub, C.B., Suresh, V., Krasieva, T., *et al.* Noninvasive assessment of collagen gel microstructure and mechanics using multiphoton microscopy. Biophys J **92,** 2212, 2007.
46. Nam, S., Lee, J., Brownfield, D.G., and Chaudhuri, O. Viscoplasticity enables mechanical remodeling of matrix by cells. Biophys J **111,** 2296, 2016.
47. Ban, E., Franklin, J.M., Nam, S., *et al.* Mechanisms of plastic deformation in collagen networks induced by cellular forces. Biophys J **114,** 450, 2018.
48. Wisdom, K.M., Adebowale, K., Chang, J., *et al.* Matrix mechanical plasticity regulates cancer cell migration through confining microenvironments. Nat Commun **9,** 4144, 2018.
49. Sniadecki, N.J., Anguelouch, A., Yang, M.T., *et al.* Magnetic microposts as an approach to apply forces to living cells. Proc Natl Acad Sci U S A **104,** 14553, 2007.
50. Bement, W.M., Mandato, C.A., and Kirsch, M.N. Wound-induced assembly and closure of an actomyosin purse string in *Xenopus* oocytes. Curr Biol **9,** 579, 1999.
51. Murrell, M., Kamm, R., and Matsudaira, P. Tension, free space, and cell damage in a microfluidic wound healing assay. PLoS One **6,** e24283, 2011.
52. de la Puente, P., Quan, N., Hoo, R.S., *et al.* Newly established myeloma-derived stromal cell line MSP-1 supports multiple myeloma proliferation, migration, and adhesion and induces drug resistance more than normal-derived stroma. Haematologica **101,** e307, 2016.
53. Wang, W.Y., Davidson, C.D., Lin, D., and Baker, B.M. Actomyosin contractility-dependent matrix stretch and recoil induces rapid cell migration. Nat Commun **10,** 1186, 2019.

Address correspondence to:
Christopher Moraes, PhD
Department of Chemical Engineering
McGill University
3610 University Street
Montreal, QC, H3A 0C5
Canada

E-mail: chris.moraes@mcgill.ca

Received: May 2, 2019
Accepted: July 9, 2019
Online Publication Date: September 20, 2019